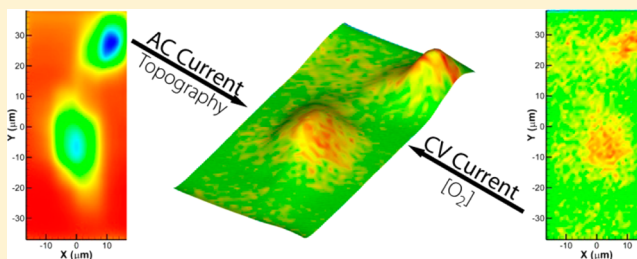


Alternating Current Scanning Electrochemical Microscopy with Simultaneous Fast-Scan Cyclic Voltammetry

Jason A. Koch,^{†,§} Melinda B. Baur,[‡] Erica L. Woodall,[‡] and John E. Baur^{*,†}[†]Department of Chemistry, Illinois State University, Normal, Illinois 61790-4160, United States[‡]Department of Chemistry, Illinois Wesleyan University, Bloomington, Illinois 61701, United States

S Supporting Information

ABSTRACT: Fast-scan cyclic voltammetry (FSCV) is combined with alternating current scanning electrochemical microscopy (AC-SECM) for simultaneous measurements of impedance and faradaic current. Scan rates of 10–1000 V s^{−1} were used for voltammetry, while a high-frequency (100 kHz), low-amplitude (10 mV rms) sine wave was added to the voltammetric waveform for the ac measurement. Both a lock-in amplifier and an analog circuit were used to measure the amplitude of the resultant ac signal. The effect of the added sine wave on the voltammetry at a carbon fiber electrode was investigated and found to have negligible effect. The combined FSCV and ac measurements were used to provide simultaneous chemical and topographical information about a substrate using a single carbon fiber probe. The technique is demonstrated in living cell culture, where cellular respiration and topography were simultaneously imaged without the addition of a redox mediator. This approach promises to be useful for the topographical and multidimensional chemical imaging of substrates.



Scanning electrochemical microscopy (SECM) normally relies on the use of a redox mediator to provide information about a substrate. Redox mediators are frequently not desired, however, because they can have deleterious interactions with the substrate. Many conventional redox mediators, for example, can be toxic to living substrates.^{1–5} Several techniques have been developed to provide information about the substrate without the use of redox mediators while allowing simultaneous electrochemical measurements. Shear force based SECM,^{6–12} alternating current SECM (AC-SECM),^{12–19} and atomic force microscopy–SECM (AFM–SECM)^{20–23} are the most prominent examples of such techniques.

The combination of fast-scan cyclic voltammetry (FSCV) or fast-scan anodic stripping voltammetry (FSASV) with SECM can provide selective chemical information about processes occurring at a substrate.^{24–26} FSCV is a powerful tool for multicomponent detection in biological systems, whereas FSASV is useful for detection of multiple metal ions. When combined with SECM, however, these rapid scan techniques are not useful for providing tip–substrate distance data because they create a much smaller diffusion layer at the probe than the steady-state amperometric techniques often used in SECM. As a result, the probe has to be positioned close to the substrate using conventional amperometric feedback techniques before using the fast-scan techniques with SECM.^{24–26} Furthermore, although the chemical information is distance-dependent, the voltammetry data contain no distance (topographical) information. The combination of fast scanning techniques with AC-SECM has the potential to provide such distance

information, and even distance control, providing that the ac and the fast-scan techniques do not interfere. Such a combination promises to improve the quality of FSCV/SECM or FSASV/SECM measurements by either providing topographical information, which can then be related to the chemical information obtained, or by permitting the use of constant-distance imaging, where the constant tip–substrate separation distance simplifies the data interpretation.

In this work we describe the combination of FSCV with constant-height AC-SECM. Instrumental conditions are found under which the resulting FSCV and ac currents do not interfere, and then simultaneous chemical measurements and topographical measurements are made without a redox mediator. This combined technique promises to be especially useful for biological substrates and has the potential for providing multidimensional chemical information and topography at a single, conventional probe.

■ EXPERIMENTAL SECTION

Instrumentation. The SECM used was based upon a previously described instrument.^{4,26} The block diagram of the instrumental configuration in Figure 1 shows the modifications necessary for FSCV/AC-SECM. In the simplest configuration, a 100 kHz 10 mV rms sine wave generated by the lock-in amplifier (model SR830, Stanford Research Systems) was applied to the input of a bipotentiostat having an internal

Received: August 19, 2012

Accepted: October 1, 2012

Published: October 1, 2012



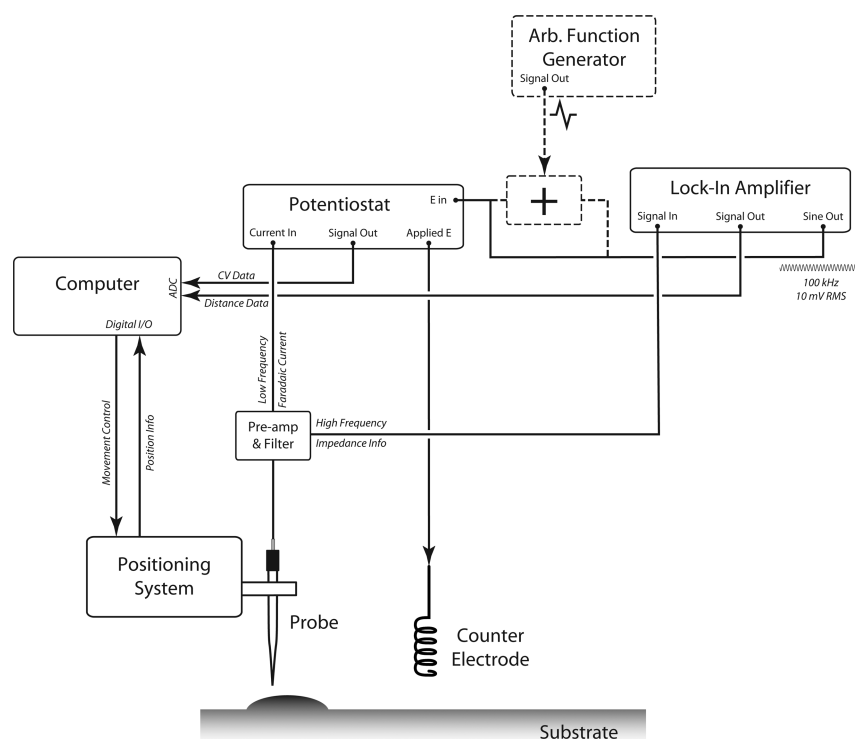


Figure 1. Block diagram of the instrumental configuration for FSCV/AC-SECM using a lock-in amplifier for the generation and measurement of the ac signal.

triangle wave generator (model EI-400, Ensman Instruments). The sum of the ac and triangle waveforms was then applied by the bipotentiostat. When a multisegment triangle wave was required for FSCV, it was generated by an arbitrary function generator (model 33220A, Agilent) which was then added to the ac waveform via a simple operational amplifier adder circuit (noninverting and unity gain). This configuration is represented by the dashed lines in Figure 1. In both configurations the computer triggered the FSCV waveform at each xyz location, but the ac waveform was continuously applied throughout the experiment.

The resulting probe current was separated into high-frequency ac (impedance) and low-frequency (faradaic current) components using a combined preamplifier and filter previously described.²⁷ The circuit had a cutoff frequency of 1.6 kHz for the high-pass filter (for AC-SECM) and 31 kHz for the low-pass filter (for voltammetry). These values adequately separated the high-frequency and low-frequency signals while causing minimal distortion to the fast-scan voltammograms (vide infra). The FSCV and ac signals were recorded as a function of xyz position and displayed (offline) using the CITS module of the scanning probe image processor (SPIP, Image Metrology).

An alternate instrumental configuration in which an analog circuit replaced the lock-in amplifier is detailed in the Supporting Information. Briefly, the circuit detects the amplitude of the current resulting from the ac waveform using a high-pass filter to remove dc and low-frequency signals, an absolute value and low-pass filter circuit to rectify the resulting high-frequency sine wave, and an amplifier to scale the output signal. The advantages of this circuit are that it can be used at higher frequencies than the lock-in amplifier (up to 400 vs 100 kHz for the lock-in amplifier) where the capacitive reactance contributions to the impedance signal are diminished and it is a much lower-cost alternative to the lock-in amplifier.

However, the bandwidth of this circuit is significantly greater than that of the lock-in amplifier, resulting in a somewhat noisier signal. Block diagrams, circuit schematics, and instrument characterization data are available in the Supporting Information.

Electrochemical Methods. Carbon fiber electrodes were made from 7 μm diameter fibers (Thornel T650, Cytec Industries) and beveled at 90° on a diamond polishing wheel (model BV-10, Sutter Instrument Company).²⁸ The platinum substrate electrode was made by sealing a 10 μm diameter platinum wire (Goodfellow) in glass and polishing with alumina (Buehler) to a mirror finish. Voltammetric measurements were conducted with the bipotentiostat in the three-electrode mode, with a platinum wire auxiliary electrode and a Ag/AgCl reference electrode (3.5 M NaCl internal solution). The potentiostat's low-pass filter was set to 20 times the scan rate used (e.g., 2 kHz for $\nu = 100 \text{ V s}^{-1}$). An RC dummy cell with $R = 47 \text{ k}\Omega$ and $C = 22 \text{ pF}$ was used for instrument characterizations. These values are approximations of the solution resistance and double layer capacitance of a 7 μm carbon fiber electrode in a phosphate buffer.

For preliminary characterization experiments, a flow system was used to introduce analyte to the electrode surface. To ensure oxygen impermeability the flow system consisted of a syringe pump with glass syringes, a stainless steel loop injector that was pneumatically activated on command from the computer, and stainless steel tubing. For all experiments with the flow system, voltammograms were recorded as a function of time and the data was analyzed using TarHeel CV (R. Mark Wightman, University of North Carolina). This software allows for the background voltammograms to be subtracted from voltammograms recorded during exposure to the analyte. For FSCV/SECM experiments, FSCV images were extracted from the four-dimensional data (i vs E vs x vs y) using SPIP, and

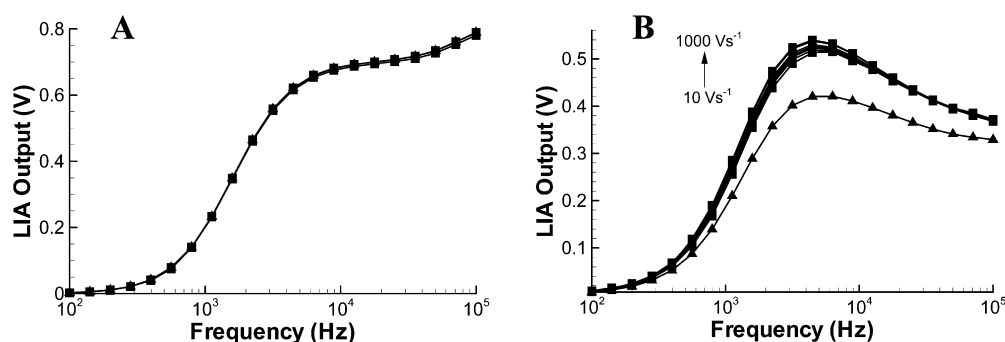


Figure 2. Frequency response of the lock-in amplifier based FSCV/AC measurement using an ac amplitude of 10 mV (rms). (A) Response for an RC “dummy cell” ($R = 47 \text{ k}\Omega$, $C = 22 \text{ pF}$) and (B) a $7 \mu\text{m}$ diameter carbon fiber microelectrode. Data were recorded with (squares) and without (triangles) a simultaneously applied triangle wave for cyclic voltammetry ($E_i = -0.400 \text{ V}$, $E_{sw} = +1.000 \text{ V}$, $\nu = 10, 20, 50, 100, 200, 500$, and 1000 V s^{-1}).

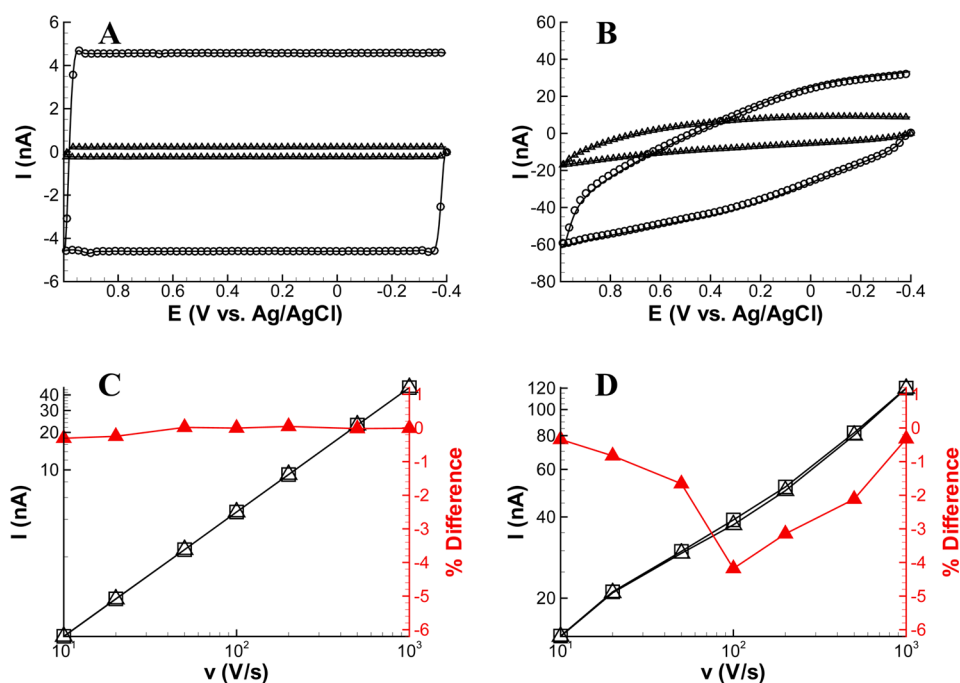


Figure 3. Background voltammograms of (A) an RC dummy cell and (B) a $7 \mu\text{m}$ diameter carbon fiber microelectrode at 10 V s^{-1} (triangles) and 200 V s^{-1} (circles) recorded with (symbols) and without (solid lines) the application of an ac waveform ($f = 100 \text{ kHz}$, $V = 10 \text{ mV rms}$). Log-log plots of the average magnitude of the background current with (open triangles) and without (open squares) the application of the ac waveform as a function of scan rate for (C) an RC dummy cell and (D) a $7 \mu\text{m}$ diameter carbon fiber microelectrode. Closed triangles represent the percent difference between the current recorded with and without the ac waveform.

approach curves and line scans were extracted from three-dimensional data (i vs E vs x or d) using a spreadsheet.

Cell Culture. Rat pheochromocytoma cells (PC12, American Type Culture Collection, ATCC) were grown on collagen-coated culture dishes (Advanced Bio-Matrix) in F-12K media supplemented with 15% horse serum, 2.5% fetal bovine serum, and penicillin/streptomycin (100 IU/mL and 100 $\mu\text{g/mL}$, respectively) (ATCC). Cells were maintained in a 7% CO_2 atmosphere at 37°C for 7–10 days. Imaging experiments were carried out in pH 7.4 Hanks’ buffer (Sigma-Aldrich) with 41 mM HEPES and 4.1 mM sodium bicarbonate.

RESULTS AND DISCUSSION

Instrument Characterization. Figure 2 shows the effect of the simultaneous application of a triangle wave (for voltammetry) on the measured ac current as a function of the ac frequency. These data were recorded from 100 Hz to

100 kHz (the upper limit of the lock-in amplifier). Data is shown both for a “dummy cell” (an RC circuit with $R = 47 \text{ k}\Omega$ and $C = 22 \text{ pF}$) and for a carbon fiber electrode with and without a simultaneously applied triangle wave ($E_i = E_f = 0.0 \text{ V}$, $E_{sw} = +1.0 \text{ V}$) at scan rates from 10 to 1000 V s^{-1} . For the dummy cell (Figure 2A), the ac measurement is essentially unaffected by the application of the triangle wave and its scan rate. This is not surprising, as the resulting voltammogram for such a dummy cell has a strong dc component that should not interfere with the high-frequency ac measurement. With the carbon fiber electrode, however, there is a substantial (up to 20%) increase in the measured ac signal when the triangle wave is applied, indicating that some of the background signal is reaching the lock-in amplifier. The background current at a carbon fiber is more complex than that at a dummy cell and may include appreciable frequency components well above those of the dummy cell. It is these higher frequencies that were

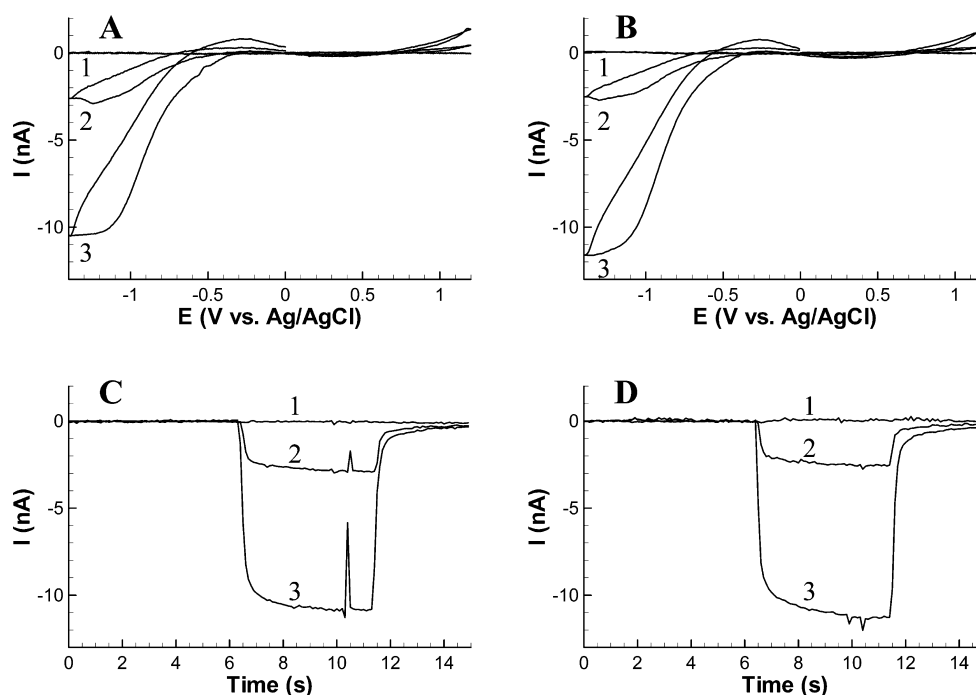


Figure 4. Fast-scan cyclic voltammetry of dissolved oxygen recorded in a flow system for a 7 μm diameter carbon fiber electrode without (A and C) and with (B and D) the application of the ac waveform. (A and B) Background-subtracted cyclic voltammograms ($\nu = 450 \text{ V s}^{-1}$) in N_2 -saturated (1), air-equilibrated (2), and O_2 -saturated (3) phosphate buffer at pH 7.4. Oxygen concentrations for these solutions are 0, 0.26, and 1.2 mM, respectively. (C and D) Average cathodic current for oxygen reduction (averaged on the cathodic scan between -1.2 and -1.3 V) as a function of time for the three solutions. Conditions: voltammetry $E_i = 0.0 \text{ V}$, $E_{\text{sw},1} = +1.2 \text{ V}$, $E_{\text{sw},2} = -1.4 \text{ V}$, $E_f = 0.0 \text{ V}$; ac waveform $f = 100 \text{ kHz}$ and $V_{\text{rms}} = 10 \text{ mV}$; carrier buffer was nitrogen-saturated phosphate buffer.

making it through the preamplifier/filter circuit to be measured as an ac current. Changing the scan rate has only a minor effect on the measured ac signal, however, indicating that these high-frequency components of the background current are not strongly dependent on the slope of the triangle wave used for cyclic voltammetry.

Figure 2A shows that for a dummy cell the optimal sensitivity for the ac measurement occurs at the maximum frequency of the lock-in amplifier (100 kHz); this is expected as the impedance of the capacitor decreases with higher frequency. These curves essentially show the high-frequency response for the high-pass preamplifier/filter circuit used for the work ($f_0 = 1.6 \text{ kHz}$). The optimal sensitivity for the carbon fiber electrode (Figure 2B), however, is about 8 kHz, after which the signal decreases slowly with frequency. This behavior differs from that previously observed at a platinum electrode²⁷ and may result from a phase change in the ac response,²⁹ as all measurements were made without adjusting the lock-in amplifier's phase. Despite the somewhat lowered sensitivity at higher frequencies, subsequent ac measurements were made at 100 kHz because at higher frequencies there were smaller differences between the measured ac signals with changes in scan rate.

Similar trends were observed for measurements made with the analog circuit in place of the lock-in amplifier (Supporting Information Figure S-2), although that configuration allows for measurements at ac frequencies higher than 100 kHz. Unlike the measurements with the lock-in amplifier, the ac responses for both the dummy cell and the carbon fiber electrode exhibit maxima (approximately 60 kHz for the dummy cell and 25 kHz for the carbon fiber electrode) and then drop toward zero as the frequency reaches 500 kHz. The advantage of the analog circuit is that it can make measurements above 100 kHz, where

lower contributions of capacitive reactance from the double layer capacitance should improve the measurement of solution impedance. As mentioned previously, however, the increased bandwidth of the circuit results in a higher noise level that offsets this advantage. Further work toward improving the noise characteristics of the circuit is therefore warranted.

The effect of the ac waveform on the cyclic voltammetry was also investigated, both in terms of the background measurements (Figure 3) and the voltammetry of dissolved oxygen (Figure 4). Background voltammograms for a dummy cell and a carbon fiber electrode were compared at various scan rates (between 10 and 1000 V s^{-1}), with and without the application of the ac waveform. For clarity, only two scan rates (10 and 200 V s^{-1}) are shown in Figure 3, parts A and B. There is close agreement between the shape and magnitudes of the background currents with (circles) and without (lines) the application of the ac waveform, although the low-pass filtering effect of the preamplifier on the faradaic current is apparent in the dampened response at the switching potential of the carbon fiber voltammograms. Parts C and D of Figure 3 compare the magnitudes of the average current for the background voltammograms at the entire range of scan rates, along with the percent difference between measurements made with and without FSCV at all scan rates. In both cases the current increases linearly with scan rate, as expected for background current. Clearly, the application of the sine wave has only a very small effect on the background voltammograms. In the worst case there is a 4% deviation (at 100 V s^{-1} at the carbon fiber electrode) in the magnitude of the current with and without the ac excitation signal, but the overall shapes of the background voltammograms are essentially unaffected.

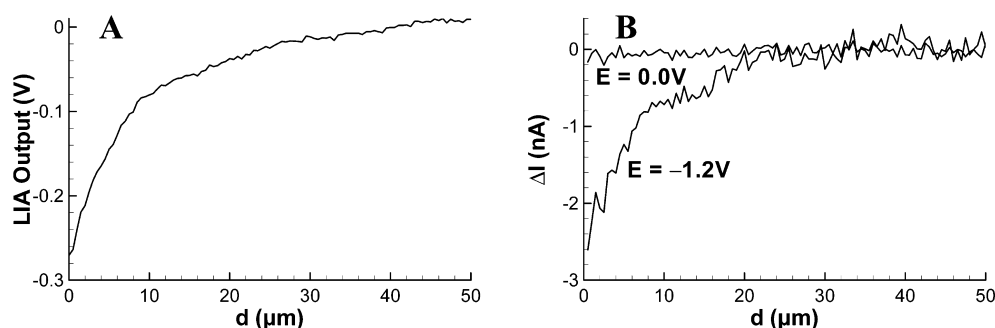


Figure 5. Simultaneous (A) ac and (B) FSCV approach curves recorded with a carbon fiber electrode approaching a 10 μm Pt substrate electrode reducing O_2 . The FSCV approach curves were extracted -1.2 V (maximum sensitivity for detection of O_2) and at a 0.0 V (no detection of O_2). ΔI represents the change in current from $d \rightarrow \infty$; a negative ΔI represents a decrease on O_2 concentration. Conditions for voltammetry and ac are the same as in Figure 4.

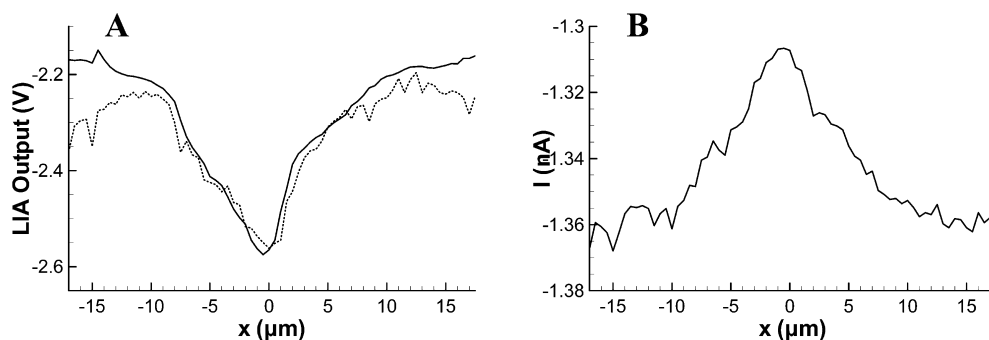


Figure 6. Constant-height line scans recorded over a living PC12 cell. (A) The ac line scans recorded either at a constant applied potential of -1.2 V (solid line) or with simultaneous FSCV (dashed line). (B) Faradaic current recorded at -1.2 V during the acquisition of the impedance signal from panel A. The presence of the respiring cell is evident by the decrease of local oxygen concentration resulting in a decrease in cathodic current near $x = 0$. Conditions for voltammetry and ac are the same as in Figure 4.

Nearly identical results were obtained with the analog circuit measurement of the ac signal (Supporting Information Figure S-3), although the variability between the background current at the carbon fiber electrode was substantially greater (13% at most). Presumably this variability arises from the large bandwidth of the analog circuit that allows some of the higher-frequency components of the voltammogram to be detected as an ac response, whereas the lock-in amplifier has a sufficiently narrow bandwidth that such effects are lower.

The carbon fiber electrode was placed in a flow system to investigate the effect of the ac measurement on the voltammetry of dissolved oxygen. Figure 4 compares the background-subtracted voltammograms of oxygen without (Figure 4A) and with (Figure 4B) the added ac waveform. Parts C and D of Figure 4 are plots of the corresponding peak currents as a function of time. The CVs recorded without the ac measurement are nearly indistinguishable from the data recorded with the ac waveform. There are small differences in the reduction current, but such differences are within the limits of variation typically observed for FSCV at carbon fiber electrodes. Combined, Figures 3 and 4 demonstrate that FSCV measurements in the presence of an ac measurement are possible without substantial degradation of the voltammetric signal.

FSCV/AC-SECM. The effect of combining FSCV with AC-SECM was also investigated. For this, we desired a test system that generated a chemical gradient but in which there would be no feedback interaction between the probe and the substrate. One such system is the oxygen gradient generated above a platinum substrate electrode set to a potential where dissolved

oxygen is reduced. Figure 5 shows FSCV and ac approach curves recorded simultaneously above this substrate. The ac approach curve in Figure 5A shows a typical negative feedback shape, as would be expected with an impedance measurement.²⁷ However, the ac signal shows occasional drift, which is evident in the slightly positive slope in the approach curve when the probe was far from the substrate. The FSCV approach curves in Figure 5B were recorded simultaneously at the cathodic peak potential for oxygen (-1.2 V) and at 0.0 V (i.e., no faradaic reaction). These approach curves are plotted as change in current relative to the current far from the substrate. The FSCV data show no sign of drift and in fact agree closely with our previous FSCV/SECM results when using a respiring cell as a substrate.²⁵

Next, we investigated the ability of the technique to image a substrate with a high relief at which a detectable chemical gradient is present. Cultured, living cells slightly diminish the oxygen level in the local environment as they respire, and the resulting oxygen gradient is measurable by SECM.³⁰ Figure 6 shows simultaneous FSCV and AC-SECM line scans recorded across a single PC12 cell with the probe operated at a constant height. Figure 6A compares ac line scans across the same cell location at a constant applied potential (solid line) and with a simultaneous FSCV measurement (dashed line). Although the ac signal with simultaneous FSCV shows a higher level of drift, the overall shapes of two line scans closely agree. The cell's respiration is detectable in the line scan shown in Figure 6B. This curve represents the reduction current measured at a constant applied potential of -1.2 V; as expected the current decreases (i.e., becomes less negative) as the probe passes over

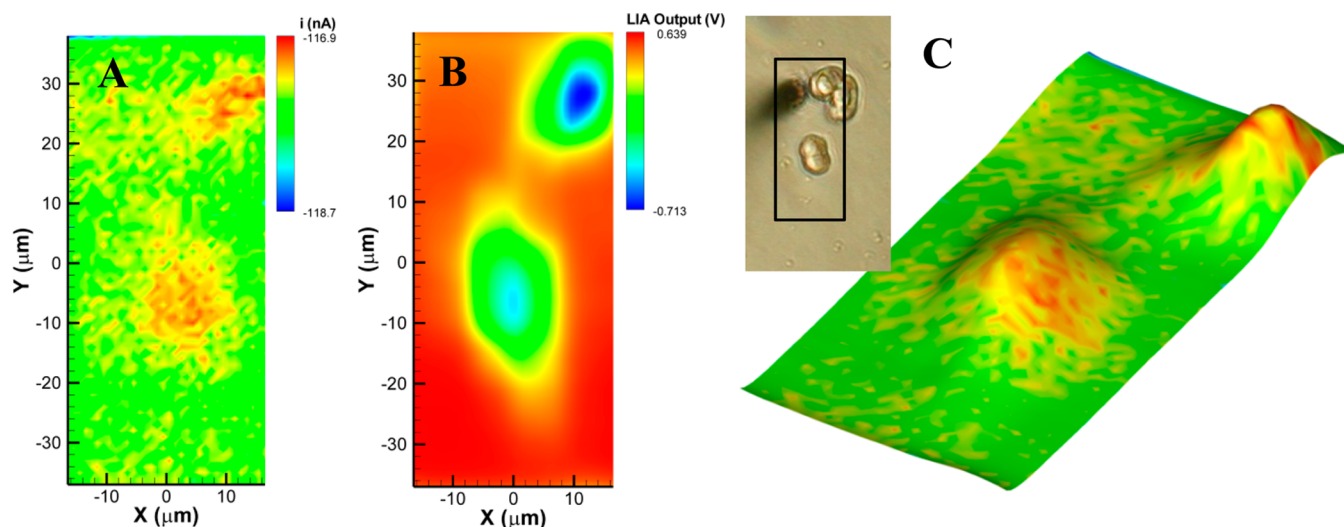


Figure 7. Simultaneous constant-height ac imaging of topography and FSCV detection of oxygen for a group of PC12 cells in Hanks' buffer with no redox mediator. (A) Cathodic current averaged at $E = -1.2$ V (the peak potential for reduction of O_2) as a function of probe position. (B) Impedance as a function of probe position, recorded simultaneously with the data from panel A. (C) Overlay of oxygen reduction current from panel A on a three-dimensional representation of the topography measured by the ac response from panel B, and an optical photograph of the two cell clusters and the carbon fiber electrode used for imaging. The SECM images were recorded in $1\ \mu\text{m}$ step sizes with a total imaging time of approximately 14 min. Conditions for voltammetry and ac are the same as in Figure 4.

the cell ($x = 0\ \mu\text{m}$). Unfortunately for this cell a measurable oxygen change could not be detected with FSCV, most likely as a result of the probe being too distant from the cell. FSCV also has a lower signal-to-noise ratio (S/N) and requires offline extraction of the signal, making it more difficult to reliably measure low oxygen levels with FSCV than with a constant potential.

Shown in Figure 7, however, is a group of cells in which the oxygen change was prominent. The FSCV oxygen signal is shown in Figure 7A, while the topography simultaneously recorded as impedance with constant-height AC-SECM is shown in Figure 7B. The oxygen signal is overlaid on a three-dimensional representation of the topography (i.e., the data from Figure 7B) in the center section of Figure 7. The areas of decreased oxygen concentration (red) coincide with the locations of the cells, demonstrating that cell topography and oxygen consumption can be imaged at the same time. Presently, our instrumentation has a minimum step size of $0.5\ \mu\text{m}$, but the use of smaller probes and a positioner with lower step sizes should lead to improved spatial resolution.

CONCLUSIONS

It was demonstrated that FSCV and AC-SECM can be combined to make simultaneous measurements of solution impedance and/or substrate topography. This technique increases the breadth of information that can be recorded in a single SECM experiment, as it is now possible to make chemically and spatially resolved measurements along with imaging topography. The versatility and wide applicability of FSCV promises to make its combination with AC-SECM applicable to a variety of chemical systems. Despite the relatively poor S/N of the oxygen measurements, however, these data demonstrate that simultaneous chemical and topographical measurements are possible and that improvements in circuitry, noise reductions, and improved data processing will make it possible to use the power of FSCV to carry out multicomponent chemical imaging simultaneously with topographical imaging. Furthermore, the ability to do this

in a solution without an added mediator, and even in cell growth media, means it will make it useful for long-term topographical and chemical measurements during cell growth and degeneration.

ASSOCIATED CONTENT

Supporting Information

Block diagrams of the instrumental configuration, characterization data for the analog circuit for the AC-SECM measurements, and a schematic diagram of this circuit. This material is available free of charge via the Internet at <http://pubs.acs.org>.

AUTHOR INFORMATION

Corresponding Author

*Phone: 309-438-7661. E-mail: jebaur@ilstu.edu.

Present Address

[§]Department of Chemistry, University of Michigan, Ann Arbor, Michigan 48109.

Notes

The authors declare no competing financial interest.

ACKNOWLEDGMENTS

This work was partially supported by an Artistic and Scholarly Development grant from Illinois Wesleyan University.

REFERENCES

- (1) Bergner, S.; Wegener, J.; Matysik, F.-M. *Anal. Chem.* **2010**, *83*, 169–174.
- (2) Bergner, S.; Wegener, J.; Matysik, F.-M. *Anal. Methods* **2012**, *4*, 623–629.
- (3) Li, X.; Bard, A. J. *J. Electroanal. Chem.* **2009**, *628*, 35–42.
- (4) Liebetrau, J. M.; Miller, H. M.; Baur, J. E.; Takacs, S. A.; Anupunpisit, V.; Garriss, P. A.; Wipf, D. O. *Anal. Chem.* **2003**, *75*, 563–571.
- (5) Petersen, N. O.; Ding, Z.; Zhao, X. *Can. J. Chem.* **2007**, *85*, 175–183.

- (6) Ballesteros, K. B.; Schulte, A.; Schuhmann, W. *Chemistry* **2003**, *9*, 2025–2033.
- (7) Cougnon, C.; Bauer-Espindola, K.; Fabre, D. S.; Mauzeroll, J. *Anal. Chem.* **2009**, *81*, 3654–3659.
- (8) Etienne, M.; Anderson, E. C.; Evans, S. R.; Schuhmann, W.; Fritsch, I. *Anal. Chem.* **2006**, *78*, 7317–7324.
- (9) Lee, Y.; Ding, Z.; Bard, A. J. *Anal. Chem.* **2002**, *74*, 3634–3643.
- (10) Nebel, M.; Eckhard, K.; Erichsen, T.; Schulte, A.; Schuhmann, W. *Anal. Chem.* **2010**, *82*, 7842–7848.
- (11) Schulte, A.; Nebel, M.; Schuhmann, W. *Methods Enzymol.* **2012**, *504*, 237–254.
- (12) Takahashi, Y.; Shiku, H.; Murata, T.; Yasukawa, T.; Matsue, T. *Anal. Chem.* **2009**, *81*, 9674–9681.
- (13) Kurulugama, R. T.; Wipf, D. O.; Takacs, S. A.; Pongmayteegul, S.; Garriss, P. A.; Baur, J. E. *Anal. Chem.* **2005**, *77*, 1111–1117.
- (14) Katemann, B. B.; Schulte, A.; Calvo, E. J.; Koudelka-Hep, M.; Schuhmann, W. *Electrochem. Commun.* **2002**, *4*, 134–138.
- (15) Etienne, M.; Schulte, A.; Schuhmann, W. *Electrochem. Commun.* **2004**, *6*, 288–293.
- (16) Eckhard, K.; Shin, H.; Mizaikoff, B.; Schuhmann, W.; Kranz, C. *Electrochem. Commun.* **2007**, *9*, 1311–1315.
- (17) Eckhard, K.; Schuhmann, W. *Analyst* **2008**, *133*, 1486–1497.
- (18) Eckhard, K.; Kranz, C.; Shin, H.; Mizaikoff, B.; Schuhmann, W. *Anal. Chem.* **2007**, *79*, 5435–5438.
- (19) Diakowski, P. M.; Ding, Z. *Phys. Chem. Chem. Phys.* **2007**, *9*, 5966–5974.
- (20) Macpherson, J. V.; Unwin, P. R. *Anal. Chem.* **2001**, *73*, 550–557.
- (21) Macpherson, J. V.; Unwin, P. R. *Anal. Chem.* **2000**, *72*, 276–285.
- (22) Kueng, A.; Kranz, C.; Lugstein, A.; Bertagnolli, E.; Mizaikoff, B. *Angew. Chem., Int. Ed.* **2003**, *42*, 3238–3240.
- (23) Kranz, C.; Friedbacher, G.; Mizaikoff, B.; Lugstein, A.; Smoliner, J.; Bertagnolli, E. *Anal. Chem.* **2001**, *73*, 2491–2500.
- (24) Alpuche-Aviles, M. A.; Baur, J. E.; Wipf, D. O. *Anal. Chem.* **2008**, *80*, 3612–3621.
- (25) Schrock, D. S.; Baur, J. E. *Anal. Chem.* **2007**, *79*, 7053–7061.
- (26) Schrock, D. S.; Wipf, D. O.; Baur, J. E. *Anal. Chem.* **2007**, *79*, 4931–4941.
- (27) Alpuche-Aviles, M. A.; Wipf, D. O. *Anal. Chem.* **2001**, *73*, 4873–4881.
- (28) Kelly, R. S.; Wightman, R. M. *Anal. Chim. Acta* **1986**, *187*, 79–87.
- (29) Serac, A. S.; Ates, M.; Kilic, B. *Int. J. Electrochem. Sci.* **2008**, *3*, 777–786.
- (30) Takii, Y.; Takoh, K.; Nishizawa, M.; Matsue, T. *Electrochim. Acta* **2003**, *48*, 3381–3385.